actuators

MDPI

Article

Robust Tracking Control of Piezo-Actuated Nanopositioning Stage Using Improved Inverse LSSVM Hysteresis Model and RST Controller

Ayad G. Baziyad *, Irfan Ahmad, Yasser Bin Salamah and Abdulaziz Alkuhayli

Department of Electrical Engineering, College of Engineering, King Saud University, Riyadh 11421, Saudi Arabia
* Correspondence: ayadgaafar@gmail.com

Abstract: Nanopositioning technology is widely used in high-resolution applications. It often uses piezoelectric actuators due to their superior characteristics. However, piezoelectric actuators exhibit a hysteresis phenomenon that limits their positioning accuracy. To compensate for the hysteresis effect, developing an accurate hysteresis model of piezoelectric actuators is very important. This task is challenging, requiring some considerations of the multivalued mapping of hysteresis loops and the generalization capabilities of the model. This challenge can be dealt with by developing a machine learning-based model, whose inverse model can be used to efficiently design an accurate feedforward controller for hysteresis compensation. However, this approach depends on model accuracy and the type of data used to train the model. Thus, accurate prediction of the hysteresis behavior may not be guaranteed in the presence of disturbances. In this paper, a machine learning-based model is used to design a hysteresis compensator and then combined with a robust feedback controller to enhance the robustness of a nanopositioning control system. The proposed model is based on hysteresis operators, the least square support vector machine (LSSVM) method, and particle swarm optimization (PSO) algorithm. The inverse model is used to design the feedforward controller, and the RST controller is employed to develop feedback control. Our main contribution is the introduction of a hybrid controller capable of compensating for the hysteresis effect, and at the same time, eliminating remaining modeling errors and rejecting disturbances. The performance of the proposed approach is evaluated through MATLAB simulation, as well as through real-time experiments. The experimental results of our approach demonstrate superior tracking performance compared with the PID-LSSVM controller.

Keywords: nanopositioning systems; piezoelectric actuators; RST controller; least-squares support-vector machine (LSSVM); hysteresis modeling; control

Citation: Baziyad, A.G.; Ahmad, I.; Salamah, Y.B.; Alkuhayli, A. Robust Tracking Control of Piezo-Actuated Nanopositioning Stage Using Improved Inverse LSSVM Hysteresis Model and RST Controller. *Actuators* **2022**, *11*, 324. https://doi.org/10.3390/act11110324

Academic Editor: Katsushi Furutani

Received: 29 September 2022
Accepted: 2 November 2022
Published: 7 November 2022

1. Introduction

Nanopositioning technology is very important in many applications that require ultra-precise motion. Such applications typically use nanopositioners to achieve their desired performance. The piezoelectric actuator is one of the fine positioning devices that is widely used in many nanopositioning systems due to its superior characteristics, such as high resolution, high output force, and fast response, compared with conventional actuators. However, the hysteretic behavior of piezoelectric actuators is a major obstacle that reduces their performance. Hysteresis is characterized by a complex nonlinear map [1], so it is hard to establish an accurate model and practical control of piezoelectric actuators [2].

To obtain a more accurate model of the piezoelectric actuator, multivalued hysteresis mapping should first be properly transformed into a one-to-one mapping, so that it does not affect modeling performance. It is also important to develop a generalized modeling algorithm to accurately describe both rate-independent and rate-dependent hysteresis [3]. Rate-dependent hysteresis is more difficult to model than rate-independent, as its response

depends not only on the input amplitude but also on the input frequencies [4,5]. Conventional hysteresis models can only characterize rate-dependent hysteresis, such as the Prandtl–Ishlinskii (PI) model [6], Bouc–Wen model [7], Duhem model [8], and Preisach model [9]. Some studies have improved these models to describe both types of hysteresis [10–12]. However, they are complex, and their inverse model often cannot be used for ultra-high precision control.

Consequently, artificial neural networks (ANNs) have been used to obtain an applicable inverse model. Although ANN-based models have addressed the computational complexity issues and introduced an appropriate nonlinear input-output mapping [13–15], they often suffer from overfitting, as they are prone to falling into local optimums, which affects their generalization ability [16]. To avoid this effect, the least-squares support vector machine (LSSVM) [17] has been used. In general, LSSVM is superior to and more accurate than ANNs, as it can reduce the upper bound of the generalization error, whereas ANNs can only minimize the training error [18]. As LSSVM only deals with one-to-one mapping, whereas hysteresis is defined as multi-valued, few studies have attempted to provide a suitable hysteresis map, often based on expanding input space into multidimensional space. For instance, the authors in [19–22] used nonlinear autoregressive exogenous (NARX) models in which the input was expanded to include current and past inputs, as well as the past outputs. Although the results showed that the outputs could be well-predicted, the output of the inverse LSSVM-NARX model that is fed to its input usually results in accumulated errors over time [23,24].

Farrokh in [24] presented a rate-dependent hysteresis model for magnetostrictive actuators using hysteresis memory and a LSSVM-based learning algorithm. The stop operators were used to construct a discrete memory to solve mapping problems, and the LSSVM was used to accurately estimate the density function. This model provided a complete memory for hysteresis and could avoid the accumulation of feedback errors caused by the LSSVM-NARX model. However, the performance evaluation of both hysteresis modeling and control has only been conducted through MATLAB simulation. Although the results have outperformed those obtained by the ANN and LSSVM-NARX models with better modeling accuracy, practical control issues were not investigated in his study.

In a previous study [25], we improved the learning and generalization capabilities of the same model (LSSVM and stop operators) using the particle swarm optimization (PSO) technique. We also evaluated its inverse as a feedforward controller for a piezoelectric stack actuator, and examined the practical issues associated with implementing our control scheme. A trade-off between the positioning accuracy and complexity was performed, which was directly affected by the number of stop operators. The inverse LSSVM model and PID controller were used in a parallel control structure to achieve high positioning accuracy with reasonable computational complexity. Further improvements in the accuracy of this scheme can be made using several stop operators, but this would be at the expense of a longer execution time. Furthermore, adjustment of PID parameters for this scheme should be carefully tuned through experiments. This task depends on a trial-and-error method, which takes a long time to reach the desired level of performance, making the choice of PID controller parameters difficult.

In this study, in continuation of our previous work, we extended the feedforward-feedback control scheme to track the same excitation signals with higher accuracy so that it would not add further complexity to the control system. Instead of the traditional feedback control, proper robust control was used to design the control scheme. This was done to deal with the uncertainty of the system and avoid the limitations of the PID controller. The methodology of the feedback controller design considered in this study utilized a pole placement technique with shaping of the sensitivity functions [26–28]. A polynomial RST digital controller was designed in parallel with an inverse LSSVM hysteresis model. The RST controller has been successfully applied in many applications [29–32]; it uses polynomial functions R and S to create robust feedback control components and the polynomial T in the feedforward path to improve tracking performance. The most interesting

aspect of this paper was the ability to reduce tracking error by imposing certain constraints on the shape of the closed-loop sensitivity functions. These constraints, as well as the desired closed-loop poles, helped to ensure a high degree of control under disturbances while maintaining the stability of the system. To the best of our knowledge, this control structure has never been evaluated through real-time experiments on a piezo-actuated nanopositioning system. For performance evaluation, the tracking performance of the extended control scheme was compared with that obtained from our previous work, which was based on the inverse LSSVM model and PID controller. The contributions of this study are listed below:

1. We present a new control structure to demonstrate the capability of the RST controller combined with inverse LSSVM model-based control to reject disturbances and further improve the robustness of the design.
2. We evaluate the proposed control scheme using a nanopositioning platform and provide a comparison with the results from our previous work.

The paper is organized as follows: Section 2 gives an overview of the hardware and software environments used in our study and describes the hysteresis loops obtained by different excitation signals; Section 3 describes the proposed model structure; Section 4 presents the considered control design based on the inverse LSSVM-based model and RST controller; Section 5 discusses modeling and experimental results; and Section 6 concludes the study with future research directions.

2. Hardware, Software, and Data Description

Data is usually prepared before being introduced to the model. In this study, the training and testing data were generated by exciting a piezoelectric stack actuator with different input signals on a nanopositioning platform. This section describes the main components of the experimental setup and obtained experimental data.

2.1. Hardware and Software Description

We used a platform consisting of six major components: four hardware and two software. Details of each component are discussed below and illustrated in Figure 1.

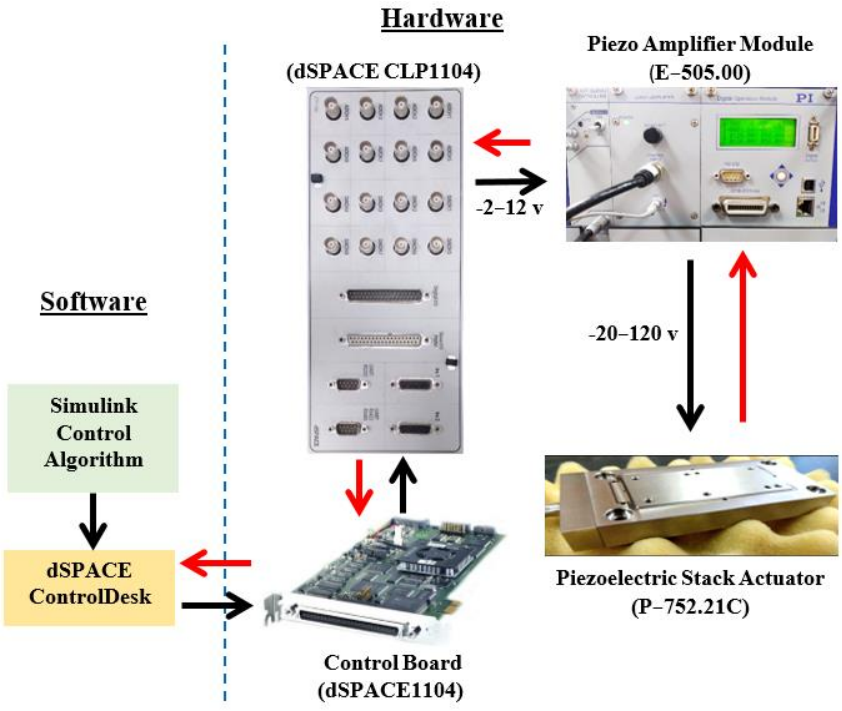

Figure 1. Hardware and software workflow.

Hardware Components: A high-speed nanopositioner stage (P-752.21C) was used to provide precise motion in a single axis, manufactured by Physik Instrumente Company, Germany [33]. This stage contained a piezoelectric stack actuator made of a ceramic material (PICMA® P-885), which could precisely expand and contract, forcing flexures to move along the desired axis. This actuator could be excited by an applied voltage ranging from −20 to 120 V, within a travel range of up to 35 µm, and a displacement resolution of 0.1 nm. To measure the output displacement, the stage was equipped with a high-resolution capacitive position sensor (D-015), which had a bandwidth of up to 10 kHz and a resolution of 0.01 nm. This sensor gave analog outputs in the voltage range of 0–10 V. To drive the piezoelectric actuator, a voltage piezo amplifier module (E-505.00) [34], from Physik Instrumente Company, Germany, was used. This module had a fixed gain of 10, and a bandwidth of 3 kHz. The operating input voltage range of this amplifier was −2 to +12 V and the output voltage response was in the range of −30 to +130 V. The input/output signals were sent from/to a control board (DS1104, dSPACE Inc, Wixom, MI, USA) [35] through a connector (dSPACE CLP1104) with 16 BNC ports. The dSPACE1104 board was used to implement control algorithms. It is well-suited for rapid prototyping and complex control systems [36–38], as it has a high-speed processor (250 MHz), 32 MB SDRAM, and 8 MB flash memory. The dSPACE1104 was directly connected to a host computer containing software packages that were used to build control models, generate C code, and visualize data.

Software: The control model was built using Simulink. The Simulink model was converted into C code with MATLAB so that it could be coupled with a dSPACE ControlDesk. The dSPACE ControlDesk was utilized for the deployment of C code on the dSPACE 1104, as well as for the visualization of the experiment results. These software packages made it possible to execute developed control algorithms on hardware-in-the-loop simulations (HILS), allowing for easy interfacing of control signals with the piezo-actuated nanopositioning systems and linking input references and output signals to visualization interfaces.

2.2. Data Description

Proper modeling of hysteresis behavior requires adequate representation of rate dependency. This is useful in examining the generalization ability of the model. Therefore, in this work, the considered actuator was driven by various input signals ranging from 1 to 20 Hz, with a sampling rate of 0.002 s. Seven excitation signals were used, three of which (A, B, and C) were used for training, and four (D, E, F, and G) that were used for testing, as shown in Figure 2. Each sub-figure shows two curves: the first curve is the input to the piezoelectric actuator (in volts) and the second curve is the output displacement of the piezoelectric actuator, measured by the capacitive position sensor (in volts). The reason for giving both curves in volts is to show input and output on the same scale to demonstrate the lag between them. It should be noted that the output responses lag the inputs. Figure 3 shows the corresponding input–output relationship, which shows the characteristics of rate-dependent hysteresis that need to be compensated by the proposed control strategy in this study. These data were then used in the modeling of the hysteretic behavior of the piezoelectric actuator and the evaluation of the proposed control approach. Table 1 shows the performance of the considered piezoelectric actuator without hysteresis compensation in terms of the root mean square of error (RMSE). Significant positioning errors (at least 0.4 µm) were observed. This performance could not meet the requirements of high-precision nanopositioning systems. Thus, it is necessary to work on developing a precise hysteresis model and control. The hysteresis modeling methods used in this study are discussed in the next section.

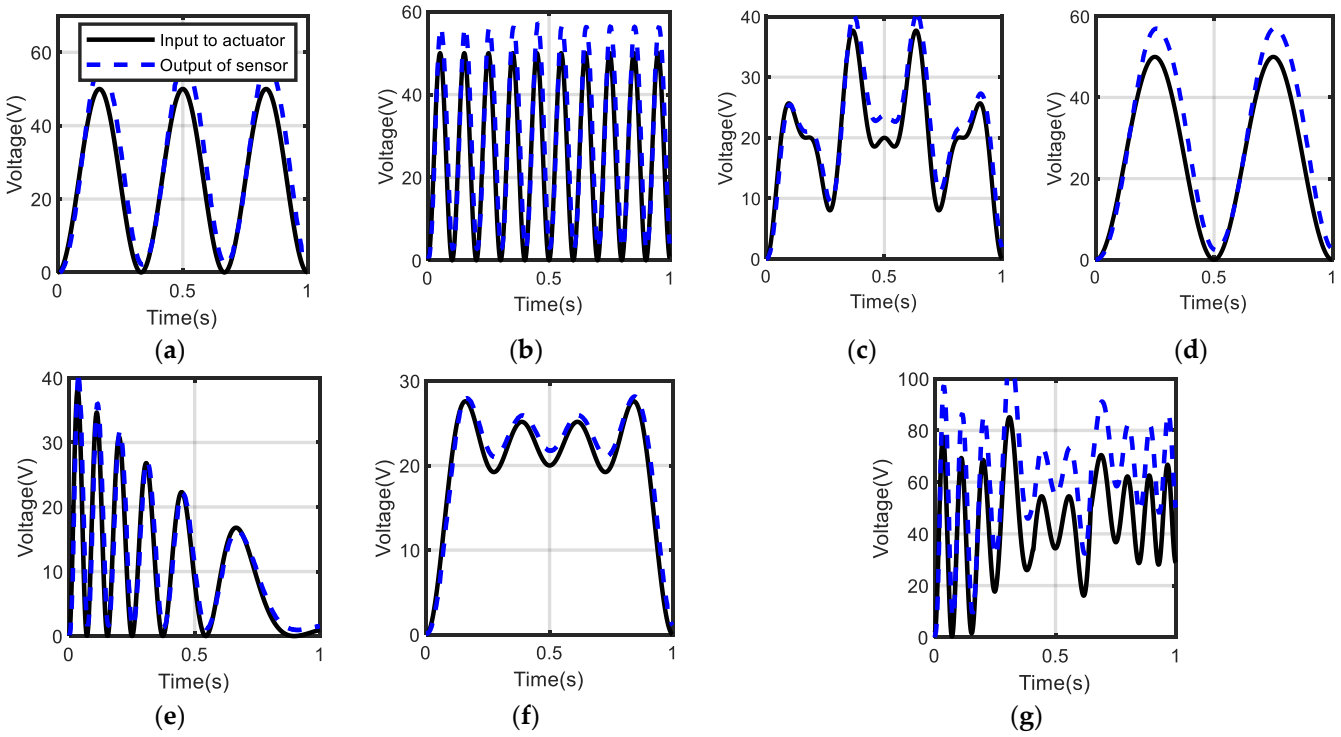

Figure 2. The lag in the output response of the actuator generated by: (**a**) input voltage A; (**b**) input B; (**c**) input voltage C; (**d**) input voltage D; (**e**) input voltage E; (**f**) input voltage F; and (**g**) input voltage G.

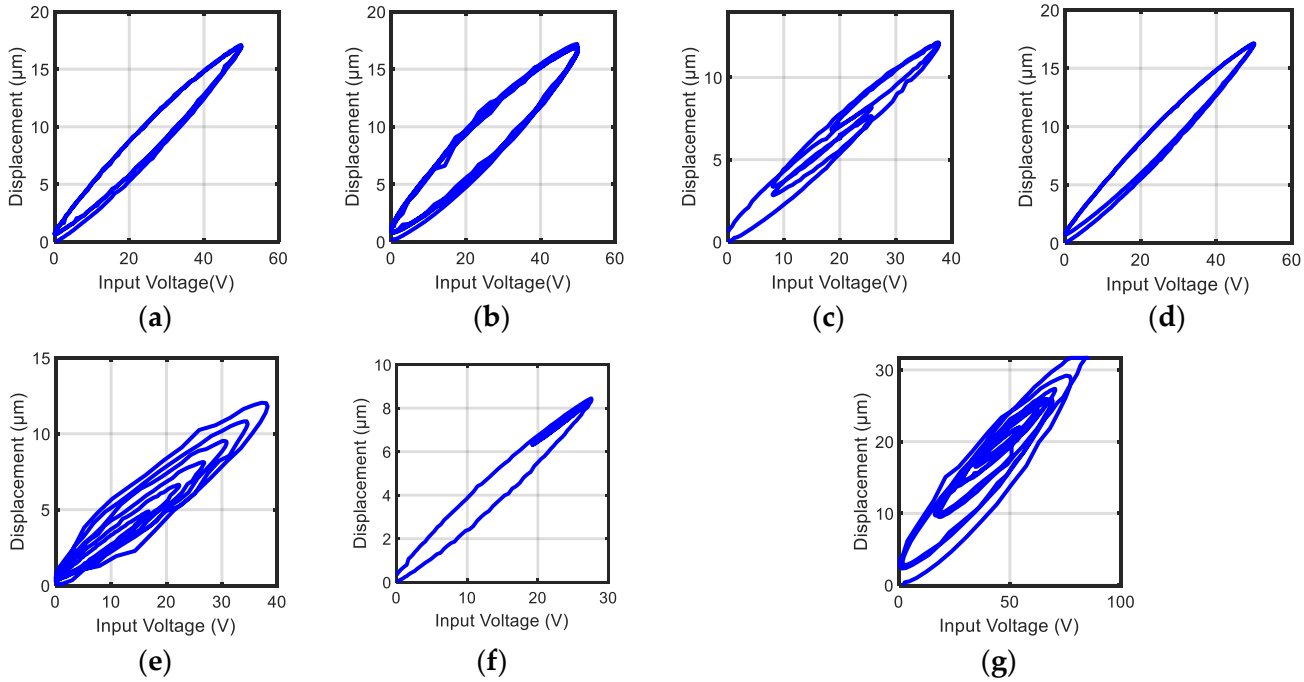

Figure 3. The corresponding input–output relationship obtained by: (**a**) reference input A; (**b**) reference input B; (**c**) reference input C; (**d**) reference input D; (**e**) reference input E; (**f**) reference input F; and (**g**) reference input G.

Table 1. Tracking performance of the considered piezoelectric actuator without hysteresis compensation.

Data	RMSE (μm)	RMSE Percentage % to Travel Range
A	1.7466	4.990%
B	2.0566	5.876%
C	0.8623	2.463%
D	1.7708	5.059%
E	0.7140	2.040%
F	0.4443	1.2695%
G	5.8008	16.5736%

The dynamic behavior of the piezoelectric actuator was not only influenced by the nonlinear hysteresis characteristics, but also by some system properties, such as stiffness and damping. The effect of system properties on the nonlinear hysteresis characteristics of the actuator was almost negligible while working at not very high frequencies. However, their effect on the overall dynamic behavior was determined in our work by identifying the system transfer function model, significantly based on the input and output data (black-box identification). Thus, the stiffness and damping properties were not individually identified in this case, but rather obtained from the information of system properties in the identified parameters of the transfer function model. For further clarification, some typical properties of the considered system are presented in Table 2.

Table 2. Typical properties of the considered piezoelectric actuator.

Properties	Values
Driven input voltage (V)	−20 to 120
Resonant frequency (Hz)	2100
Resolution (nm)	0.1
Travel range (μm)	0–35
Stage mass (kg)	0.35
Electrical capacitance (μF)	3.7
Load capacity (N)	30
Stiffness in motion direction (N/μm)	20

3. Model Structure

The proposed hysteresis model was inspired by the Preisach model [39,40]. The hysteresis behavior was described in the Preisach model using a hysteresis memory constructed by relay operators. Then, it utilized a memoryless mapping function for model identification, as demonstrated in Figure 4. The relay operator is typically defined by two thresholds, a_1 and a_2, where $a_1 \leq a_2$, as shown in Figure 5a. At these thresholds, the relay operator's output was either +1 or −1. Assuming that a voltage *z(t)* drives the piezoelectric actuator, the output can then be predicted by the Preisach model, as follows:

$$\mathrm{y(t)} = \int_0^{+\infty} \int_{-\infty}^{+\infty} \mu(r,s) R_{s-r,s+r}[z](t) ds dr \quad (1)$$

where μ represents a density or weight function and $R_{s-r,s+r}[\cdot]$ is the relay operator with center s and half-width r. This can be defined in the following formula:

$$r = (a_2 - a_1)/2 \quad (2)$$

Using a dividing curve $\psi(t,r)$, the half-plane $r > 0$ is divided into two different sections. Then, the relay takes either +1 or −1. The value −1 is assigned to the upper region of the relay, and the value +1 is assigned to the lower region. The curve $\psi(t,r)$ is called the play operator, as shown in Figure 5b, where:

$$\psi(t,r) = P_r[z](t) \; \forall r \geq 0 \quad (3)$$

Then, Equation (1) can also be expressed as:

$$\mathrm{y(t)} = \int_0^{+\infty} \left[\int_{-\infty}^{\psi(t,r)} \mu(r,s)ds - \int_{\psi(t,r)}^{+\infty} \mu(r,s)ds \right] dr \tag{4}$$

Thus, the output of the Preisach model can be predicted by the following equation:

$$y(t) = Q(r,\ \psi(t,r)) \tag{5}$$

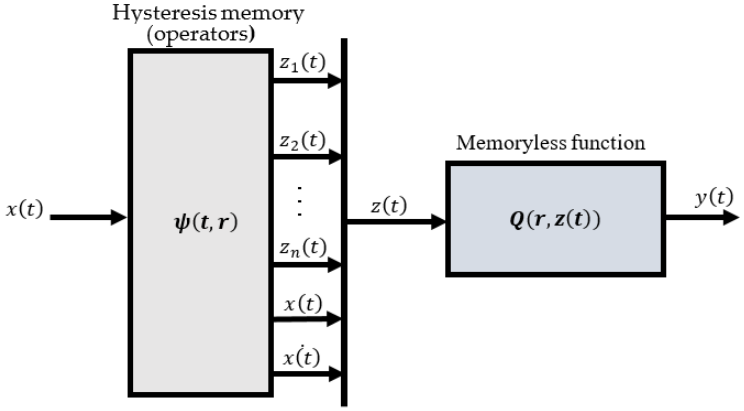

Figure 4. Schematic diagram for Preisach model.

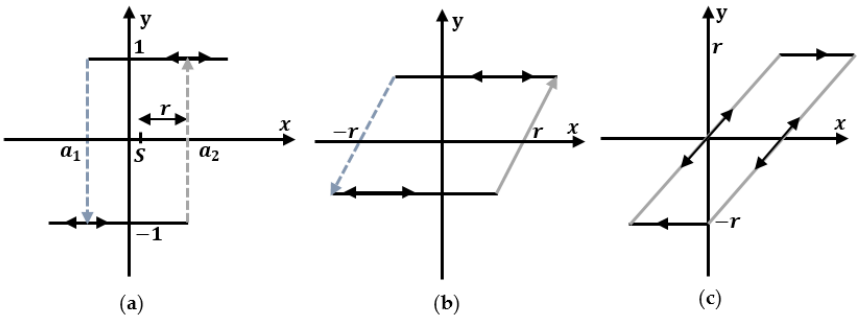

Figure 5. State transitions of Preisach operators: (**a**) relay operator; (**b**) play operator; and (**c**) stop operator.

The equation above demonstrates that the Preisach model is composed of the hysteresis play operators (hysteresis memory) and a memoryless functional mapping function. The most difficult aspect of the Preisach model is that the density function must be precisely estimated and implemented with less computational time. In this study, we used alternative hysteresis mapping and approximation strategies. The following two sections discusses the proposed modeling approach. The first section presents a discussion of the discrete hysteresis memory that was used to expand input space. The second section presents the LSSVM-based method that was used to accurately estimate the hysteresis model and explains the improved PSO algorithm that was employed to optimize the LSSVM parameters to further improve model accuracy.

3.1. Proposed Hysteresis Memory

The hysteresis memory is built in a discrete form; its plane is divided into many elements using a set of *n*-stop operators. The stop operator is characterized as shown in

Figure 5c. It has two thresholds $+r$ and $-r$ and its output for a given input $x(t)$ can be defined on the interval $[t_i, t_{i+1}]$, as follows:

$$\begin{gathered} z(0) = E_r[x(0)] \\ z(t) = E_r[x(t) - x(t_i) + z(t_i)] \\ \text{for } t_i \le t \le t_{i+1};\ 0 \le i \le N-1 \end{gathered} \tag{6}$$

where:

$$E_r[.] = min\{max\{-r, .\}, +r\} \tag{7}$$

where $z(t)$ indicates the current state of the operator and $E_r[\cdot]$ indicates the stop operator. The threshold of the stop operator is defined as:

$$r_i = \frac{i}{(n+1)|x|_{\max}},\ i = 1,\ 2,\ 3, \ldots, n \tag{8}$$

where $|x|_{\max}$ denotes the maximum absolute value and n denotes the number of operators.

3.2. Memoryless Function

In this study, the density function of the Preisach model was replaced by introducing a machine learning predictor based on the least-squares support-vector machine (LSSVM) [17,41]. This model is widely used for classification and regression as it has the capability of converting inequality constraints into equality constraints and utilizing a squared loss function that enables the LSSVM method to achieve effective linearization.

Let us assume that a piezoelectric actuator has an input z and output response y, then the LSSVM prediction model can be expressed, as follows:

$$y(z) = w^T \varnothing(z) + b \tag{9}$$

where $\varnothing(\cdot)$ is a nonlinear mapping function, w indicates the weight vector, and b is a bias term. These parameters can be optimized by training the model using a dataset with an adequate number of samples N. Then, the optimization problem can be solved by minimizing the cost function, as follows:

$$\underset{w,e,b}{min} J_p(w,e) = \frac{1}{2} w^T w + C \frac{1}{2} \sum_{k=1}^{N} e_k^2 \tag{10}$$

Equality constraints are expressed as:

$$y_k = w^T \varnothing\left(z^k\right) + b + e_k \tag{11}$$

where e_k represents error variables and C is the regularization factor that gives the relative weight to errors. The regularization parameter has a direct influence on the generalization ability of the LSSVM model; therefore, a more effective optimization should be used for better training. The optimization technique used in this study will be described later. The LSSVM algorithm usually utilizes the Lagrangian function to solve this optimization problem; thus, Equation (10) can be reformulated as follows:

$$\mathcal{L}(w, b, e; \alpha) = J_p(w, e) - \sum_{k=1}^{N} \alpha_k \left[w^T \varnothing\left(z^k\right) + b + e_k - y_k \right] \tag{12}$$

where α_k are the Lagrange multipliers. For the linear solution, the Karush–Kuhn–Tucker (KKT) conditions are used. The KKT equations are expressed as:

$$\frac{\partial L}{\partial w} = 0 \rightarrow w = \sum_{k=1}^{N} \alpha_k \varnothing\left(z^k\right) \tag{13}$$

$$\frac{\partial L}{\partial e_k} = 0 \rightarrow \alpha_k = Ce_k \tag{14}$$

$$\frac{\partial L}{\partial b} = 0 \rightarrow \sum_{k=1}^{N} \alpha_k = 0 \tag{15}$$

$$\frac{\partial L}{\partial \alpha_k} = 0 \rightarrow w^T \varnothing\left(z^k\right) + b + e_k - y_k \tag{16}$$

By substituting the KKT equations in Equation (12), the linear equations are obtained, as follows:

$$\begin{bmatrix} 0 & 1_N^T \\ 1_N & \Omega + I/C \end{bmatrix} \begin{bmatrix} b \\ \alpha \end{bmatrix} = \begin{bmatrix} 0 \\ y \end{bmatrix} \tag{17}$$

where I denotes the identity matrix, $y = [y_1, y_2, \ldots, y_N]^T$, 1_N is a unity vector, and Ω is the Gram matrix. The Gram matrix can be defined as:

$$\Omega_{kj} = K\left(z^k, z^j\right) = \varnothing\left(z^k\right)\varnothing\left(z^j\right),\ k, j\ =\ 1, 2,\ \ldots\ , N \tag{18}$$

where K denotes the kernel function. We used the radial base function (RBF) kernel, which is the most effective kernel and widely used for nonlinear regression problems. It is defined as:

$$K\left(z, z^k\right) = exp\left(-\frac{\|z - z^k\|}{\sigma^2}\right) \tag{19}$$

where σ is the kernel parameter that denotes the variance of the Gaussian function and often affects the generalization performance of the model.

Therefore, the LSSVM-based predictor can be given by:

$$\hat{y}(z) = \sum_{k=1}^{N} \alpha_k K\left(z, z^k\right) + b \tag{20}$$

Tuning the hyper-parameters C and σ^2 has a considerable impact on the accuracy of the LSSVM model. In this work, the global optimization of the LSSVM parameters was realized using the particle swarm optimization (PSO) technique, due to its intelligent searching strategy, inspired by the behavior of a flock of birds in search of food [42,43]. In the optimization process, each particle i moves in the space to find the optimal food location via inter-group communications. During every iteration t, each particle moves toward the one that is closest to the food while updating its position and velocity. This update is then shared among all the particles. This process is repeated until the best possible position is found. This can be formulated as the following:

$$\begin{gathered} v_i(t) = \eta v_i(t-1) + c_1 r_1 (p_{best,i} - p_i(t-1)) + c_2 r_2 (g_{best} - p_i(t-1)) \\ p_i(t) = p_i(t-1) + v_i(t) \end{gathered} \tag{21}$$

where $v_i(t)$ is the velocity of i^{th} particle and $p_i(t)$ is the position of i^{th} particle. The η is called the inertia weight, which is used to adjust the balance between global search and local search, g_{best} indicates the current global best, $p_{best,i}$ indicates the current personal best, c_1 is the learning factor for personal movement, c_2 is the learning factor for group movement, and r_1 and r_2 are random numbers that are uniformly selected in the range [0, 1] at each iteration. In this study, cross-validation was used to evaluate fitness on the training dataset. The flowchart of the PSO-LSSVM algorithm is presented in Figure 6.

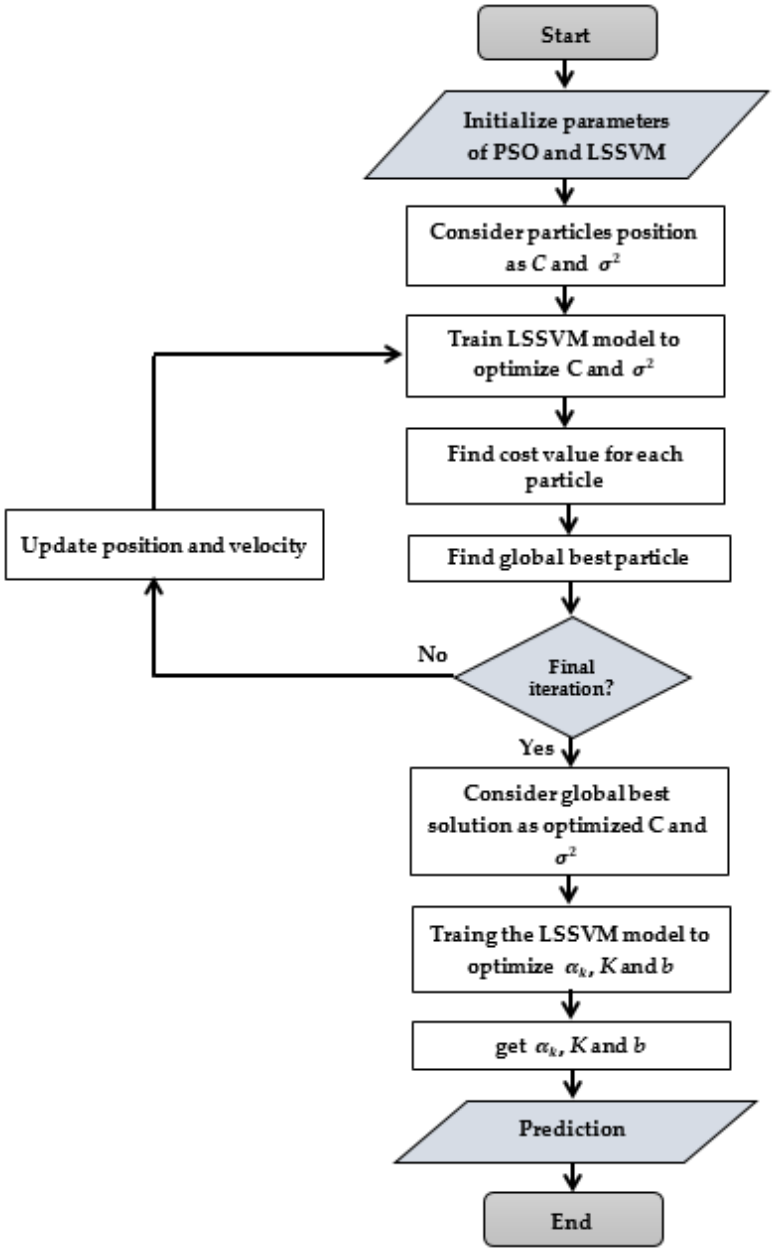

Figure 6. Flowchart of the PSO-LSSVM algorithm.

The model described above was used to fit different curves of the hysteresis loop under different excitation amplitudes and frequencies. The numerical simulation results for the performance of the model will be given and discussed in detail in Section 5 of this paper.

4. Control Design

In a previous study, we proposed a control methodology based on a kernel-based learning method for hysteresis compensation. However, its success significantly depended on a sufficient amount of representative training data and adjustment of the optimal parameters to get an adequate approximation of piezoelectric actuator behavior. As rate-dependent hysteresis is quite sensitive to disturbance, the accurate prediction of the hysteresis behavior may not be guaranteed at increasingly strong disturbances, which can affect the overall control performance. The solution to typically used address this problem is to insert a

robust feedback controller into the control loop to form a hybrid control structure capable of handling such disturbances and internal uncertainties.

For this purpose, a parallel controller structure consisting of an inverse LSSVM controller and an RST controller was proposed in this paper, as shown in Figure 7. The input control signal for the piezoelectric actuator was generated by summing two commands: a feedforward command generated by the inverse model and feedback command generated by the RST controller. According to a previous study [44], it was found that the use of RST in parallel with inverse feedforward control could efficiently control different nonlinear processes with more precise motion tracking than the cascade control structure. In addition, the inverse feedforward controller, based on the LSSVM model, may not guarantee accurate convergence of the output to the reference in the cascade control structure. This is because the outputs of the RST controller are given as inputs to the inverse model, whereas the inverse LSSVM model is usually trained by the desired displacement values. The RST controller is well-suited to be combined with our approach because of its simple structure, fast response, and insensitivity to disturbances [27]. Therefore, this approach integrates the advantages of the LSSVM-based controller, which allows high modeling accuracy for piezoelectric hysteresis, and the RST controller, which helps to overcome disturbances and enhances the robustness of tracking. The details of the inverse model and RST controller are presented in the coming sections.

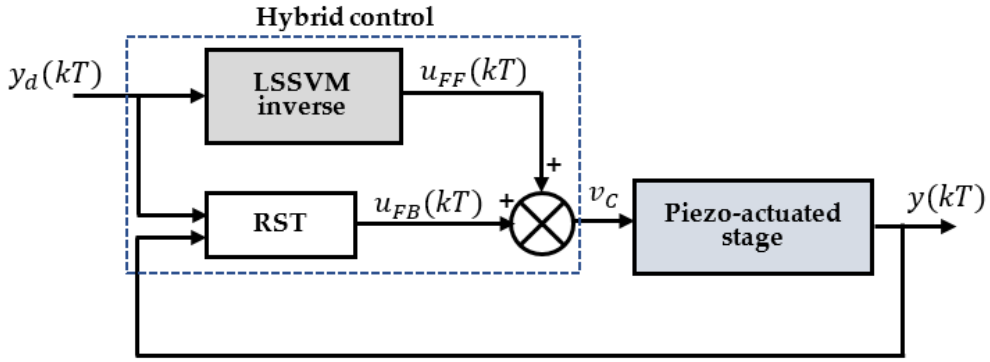

Figure 7. Proposed feedback–feedforward control structure.

4.1. Inverse LSSVM Hysteresis Model

Although inverse model compensation has been widely used to control piezoelectric actuators [45], finding the exact inverse of a hysteresis model is often challenging [3,46]. This is because it significantly depends on the efficiency of the algorithm of the hysteresis model and its ability to describe different types of hysteresis loops. Moreover, the algorithms that can provide accurate models may be too complicated to be implemented in real time. The advantage of the PSO-LSSVM method based on stop operators is that it exhibits high precision compared with other hysteresis modeling methods [22,25], and its inverse model is easy to obtain. In this study, the PSO-LSSVM algorithm was used to develop the inverse hysteresis model. The LSSVM inverse model was inversely trained with offline datasets (A, B, and C). During offline training, the output displacement was selected as the input for the LSSVM training, and the corresponding reference input as the output. After sufficient training, the LSSVM inverse model was used to produce the feedforward control signal, as shown in Figure 8. One major limitation of the LSSVM inverse model, based on hysteresis operators, was its long execution time, which occurred due to the increase in the number of operators. To avoid this issue, the order of the stop operators was set to 55 in this study, as we recommended in a previous study [25]. In this way, the size of the kernel matrix was reduced, decreasing the time complexity of the proposed control scheme. Such a compromise would guarantee the desired tracking speed and accuracy, allowing an additional feedback controller to be inserted into the control loop without more time complexity.

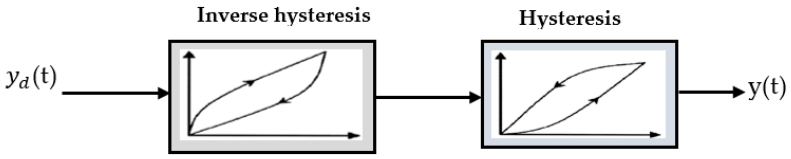

Figure 8. FF control compensation using the inverse model.

Usually, the feedforward compensator cannot eliminate the tracking error in the presence of strong disturbances. Therefore, a robust RST feedback controller was inserted into the control loop. This will be discussed in the next subsection.

4.2. RST Controller

In this study, a robust digital RST controller was combined with the feedforward controller. The RST controller usually involves the placement of a closed-loop pole with sensitivity function shaping in the frequency domain [27]. The shaping of the sensitivity functions is achieved by suitably selecting the poles of the closed-loop system, so that the desired performances in terms of tracking, disturbance rejection, and robustness are achieved. Thus, the design of the RST controller depends on the mathematical model of the piezoelectric actuator. We assume that the discrete-time transfer function for the open-loop system to be controlled is given by:

$$G(z) = \frac{B(z)}{A(z)} \tag{22}$$

The structure of the RST controller is shown in Figure 9, where R, S, and T are polynomials and constitute the RST controller $K(z)$, which can be computed as follows:

$$R\left(z^{-1}\right) = r_0 + r_1\, z^{-1} + \cdots \tag{23}$$

$$S\left(z^{-1}\right) = s_0 + s_1\, z^{-1} + \cdots \tag{24}$$

$$T\left(z^{-1}\right) = t_0 + t_1\, z^{-1} + \cdots \tag{25}$$

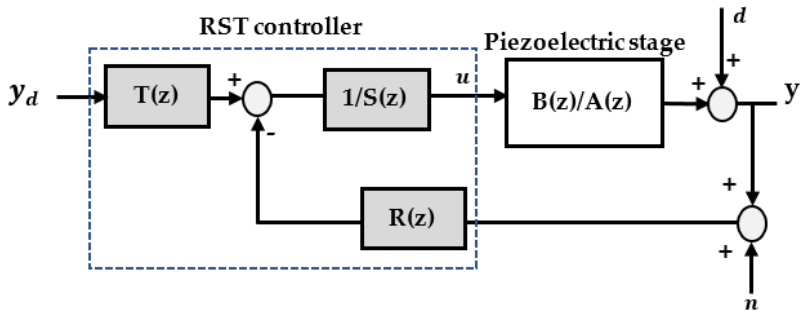

Figure 9. Structure of the RST controller.

The above equations demonstrate that the RST controller design is considered to be an optimization problem, where the coefficients of R and S have to be optimized to match the desired regulation performance. As for the polynomial T, it is made equal to a constant, where $T = R\ (1)$, which helps to ensure a steady state gain of unity between the reference and output to match the desired tracking performance. To reach the optimum solution, constraints relating to the desired performance and stability requirements of the

piezo-actuated stage were imposed on the closed loop sensitivity functions. Such sensitivity functions had the following expressions:

$$S_0\left(z^{-1}\right) = \frac{A\left(z^{-1}\right)S\left(z^{-1}\right)}{A(z^{-1})S(z^{-1}) + B(z^{-1})R(z^{-1})} \tag{26}$$

$$T_0\left(z^{-1}\right) = \frac{B\left(z^{-1}\right)T\left(z^{-1}\right)}{A(z^{-1})S(z^{-1}) + B(z^{-1})R(z^{-1})} \tag{27}$$

$$KS_0\left(z^{-1}\right) = \frac{A\left(z^{-1}\right)R\left(z^{-1}\right)}{A(z^{-1})S(z^{-1}) + B(z^{-1})R(z^{-1})} \tag{28}$$

where S_0 is the output sensitivity function, which is the transfer function between the disturbance d and the piezoelectric actuator output y; T_0 is the complementary sensitivity function, which is the transfer function between the reference y_d and the output y; and KS_0 is the input sensitivity function, which is the transfer function between the disturbance d and piezoelectric actuator input u. The constraints of these functions are given below [26]:

Constraint 1: To achieve the desired robustness, the maximum peak magnitude of S_0 needed to be less than 6 dB, $\|S_0\left(z^{-1}\right)\|_\infty < 6\ dB, \forall\omega$. This constraint helped to ensure sufficient stability margin and achieve good robustness performance.

Constraint 2: For the same reasons that "Constraint 1" was required to be imposed, the maximum peak magnitude of T_0 needed to be less than 3.5 dB, $\|T_0\left(z^{-1}\right)\|_\infty < 3.5\ dB, \forall\omega$.

Constraint 3: As the gain of the amplifier in our system was 10, the maximum peak magnitude of KS_0 needed to be less than 20 dB, $\|KS_0\left(z^{-1}\right)\|_\infty < 20\ dB, \forall\omega$, to avoid the saturation issues of the command signal.

Constraint 4: To achieve more precise tracking control, a constraint on tracking errors was required in our design. Therefore, a maximum tracking error of 0.2% of the travel range was allowed, in the range of 0–20 Hz. This constraint could be expressed by imposing a limit on the output sensitivity function, where $\left|S_0\left(z^{-1}\right)\right| < -23\ dB, 0 < \omega < \omega_T$.

The optimum solution for this problem was reached by placing the closed-loop poles within a specified region that yielded good performance under these constraints. We assumed that the closed-loop poles should be placed at desired locations, as specified by the polynomial $P\ (z^{-1})$. This polynomial was factorized to emphasize the dominant and auxiliary poles, as follows:

$$P(z^{-1}) = P_D(z^{-1})\cdot P_F(z^{-1}) \tag{29}$$

where P_D and P_F define the dominant and auxiliary poles, respectively. To find the controller polynomials R and S, the following Bizout equation needed to be solved:

$$P(z^{-1}) = A\left(z^{-1}\right)S\left(z^{-1}\right) + B\left(z^{-1}\right)R\left(z^{-1}\right) \tag{30}$$

The polynomials $R(z^{-1})$ and $S(z^{-1})$ generally contain pre-specified fixed parts, which are $H_R(z^{-1})$ and $H_s(z^{-1})$, respectively; thus, they were also factored as follows:

$$R(z^{-1}) = H_R(z^{-1})\cdot R'(z^{-1}) \tag{31}$$

$$S(z^{-1}) = H_S(z^{-1})\cdot S'(z^{-1}) \tag{32}$$

By substituting Equations (29), (31) and (32) in Equation (30), we obtain:

$$P_D(z^{-1})\cdot P_F(z^{-1}) = A\left(z^{-1}\right)H_S(z^{-1})S'\left(z^{-1}\right) + B\left(z^{-1}\right)H_S(z^{-1})R'\left(z^{-1}\right) \tag{33}$$

Therefore, the polynomials $R'(z^{-1})$ and $S'(z^{-1})$ need to be solved to design $R(z^{-1})$, $S(z^{-1})$, and $T(z^{-1})$. The design procedures of the RST controller in this paper consist of eight steps, which can be summarized as follows:

1. Estimate the transfer function of the piezoelectric stage model and obtain $B(z^{-1})$ and $A(z^{-1})$.
2. Choose dominant poles $P_D(z^{-1})$, and determine $P_F(z^{-1})$, $H_R(z^{-1})$, and $H_S(z^{-1})$.
3. From Equation (33), solve $R'(z^{-1})$ and $S'(z^{-1})$.
4. Compute $R(z^{-1})$ and $S(z^{-1})$ using Equations (31) and (32), respectively.
5. Compute $T(z^{-1})$ from the equation $T(z^{-1}) = R(1)$.
6. Compute the sensitivity functions $S_0(z^{-1})$, $T_0(z^{-1})$, and $KS_0(z^{-1})$ by Equations (26)–(28), respectively.
7. Evaluate the shaping of the sensitivity functions using the considered constraints and performance specifications.
8. Repeat steps 2 to 7 until the optimum solution is reached.

5. Results and Discussion

In this section, the performance of the proposed model and controller are discussed and compared with previous results published in [25].

5.1. Modeling Examination

In this section, the effectiveness of the proposed PSO-LSSVM model was examined. Simulations were conducted using MATLAB (version R2021b, Mathworks, Natick, MA, USA) and the LSSVMlab Toolbox (version 1.8, KU Leuven, Leuven, Belgium) [47]. The model was first trained by training data A, B, and C, and then its generalization ability to describe the rate-dependent hysteresis loops was tested by datasets D, E, F, and G. The simulations were run for both training and testing at a sample rate of 0.002 s or 500 samples per second. The maximum absolute value $|x|_{\max}$ was set to 8.5. According to a literature review [24,25], an increased number of stop operators comes at an increased computational cost, making it unsuitable for real-time implementation. This issue was investigated in our previous study [25], and we found that $n = 55$ was a good balance between computational complexity and accuracy that guaranteed significant improvement in the proposed model performance. Therefore, the same number of stop operators ($n = 55$) was applied in the present study as well.

The PSO algorithm was used to select the optimal hyper-parameters σ^2 and C of the LSSVM model. The initial parameters were set according to previous recommendations [48,49], as well as our experiments. In most practical problems, a population size of 20 to 50 achieves the best performance. The amount of 30 particles and 100 iterations was large enough to get the minimum error. The values of acceleration coefficients were suggested to be equal ($c_1 = c_2 = 2$) to achieve a balance that provided a faster convergence speed, and at the same time, enhanced the capability of escaping any local optimum to search for the global optimum. The inertia weight was set to be decreased linearly from 0.9 to 0.4. The optimum hyper-parameters obtained using the PSO algorithm were $\sigma^2 = 3.13544$ and $C = 3.8155 \times 10^3$. The model was then trained with all these parameters, and the best values for bias b and support vectors were found, as shown in Table 3.

Figure 10a–d depicts the simulation results that compare the hysteresis loops obtained from the proposed model with experimental loops. Our model performed well in modeling the rate-independent and rate-dependent hysteresis loops. The evaluation of model performance was carried out using the root mean square of error (RMSE), which measured the difference between the predicted output and experimented output. The RMSE values ranged from 0.01061 to 0.0126 μm (D = 0.01061, E = 0.01086, F = 0.0123, and G = 0.0126 μm), which indicated high prediction accuracies on all test data.

Table 3. The selected and identified hysteresis model parameters.

Parameter	Symbol	Value
Sampling rate	f_s	0.002 s
Maximum absolute input	$\|x\|_{\max}$	8.5
Stop operator order	n	55
No. of particles	n_p	30
Maximum number of iterations	i	100
Learning factors	$c_1 = c_2$	2
Inertia weights	$[w_{min}, w_{max}]$	[0.4, 0.9]
Regularization factor	C	3.8155×10^3
Kernel parameter	σ^2	3.13544
Bias	b	1.831

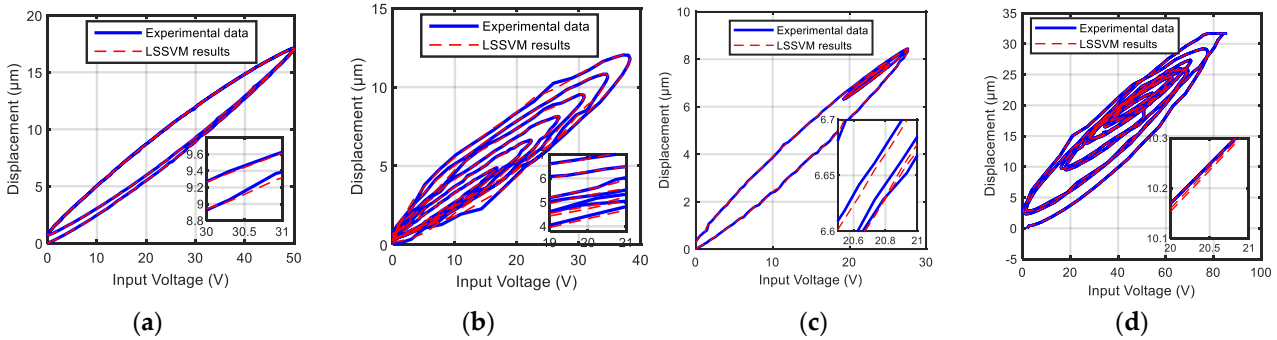

Figure 10. Simulation results of the PSO−LSSVM model on: (**a**) test data D; (**b**) test data E; (**c**) test data F; and (**d**) test data G.

Figure 11 shows the error level between the actual output of the considered piezoelectric actuator and estimated output of the proposed model. These results could be improved by increasing the number of stop operators, but this would be at the expense of model complexity. A detailed discussion about the complexity of the proposed model was given in our previous paper [25]. A comparison between our method and other hysteresis models was presented in that paper as well. The results showed that this model could achieve higher generalization performance than comparative models. As this model provides high accuracy with reasonable computation time (0.23 ms/sample), its inverse model is suitable to design a real-time compensator for the considered piezoelectric actuator.

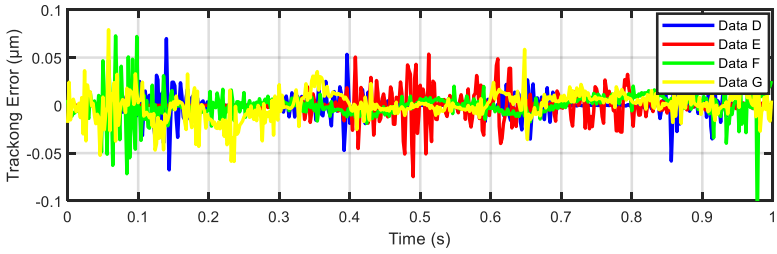

Figure 11. The error level between the actual output of the considered piezoelectric actuator and estimated output of the proposed model for test data D, E, F, and G.

5.2. Experimental Results of Reference Tracking

A hybrid controller was designed, composed of feedforward and feedback algorithms. The inverse PSO-LSSVM controller was used to compensate for hysteresis nonlinearity, whereas the RST was used to eliminate system disturbances and achieve precise tracking. To design the RST controller, a linear dynamics model $G(z)$ corresponding to the piezoelectric actuator was required. Thus, the actuator was excited by a chirp voltage signal with a small amplitude to neglect the hysteresis effect on the output response. The input and

output of the piezoelectric stage were used for open-loop identification to characterize the plant model. The parameter estimation was carried out using the recursive least squares (RLS) algorithm. The simulation results showed that a fourth-order model was suitable to characterize the linear dynamics of the considered actuator, as shown in Figure 12. It should be noted that the predicted output closely fit the actual output and the error of the fourth-order model was small, which could be handled by the robustness of the RST controller. The plant mode $G(z)$ was identified and its numerator and denominator polynomials were obtained, as follows:

$$B(z) = 0.6521z^3 - 0.80572\,z^2 + 0.3978z + 0.26 \times 10^3 \tag{34}$$

$$A(z) = z^4 - 1.646z^3 + 1.657z^2 - 1.1253z + 0.386 \tag{35}$$

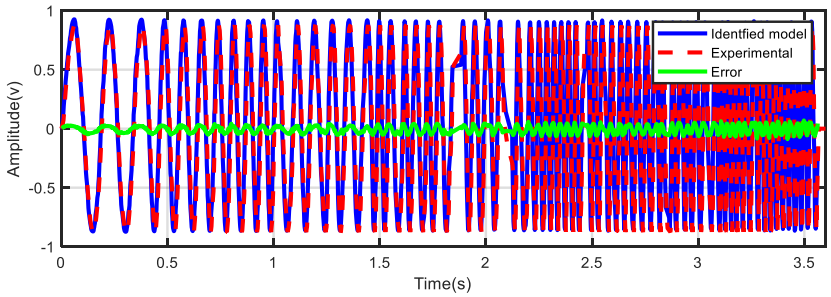

Figure 12. The fit of the actual response of the piezoelectric actuator to the simulated output of the identified transfer function.

To design the RST controller, the procedures mentioned above in Section 4.2 were followed step-by-step, and the polynomials R and S were obtained as follows:

$$\begin{aligned} R(z^{-1}) = {} & 0.247 - 0.454z^{-1} + 0.214z^{-2} + 0.479z^{-3} - 0.375z^{-4} \\ & +0.0025z^{-5} + 0.0001z^{-6} + 0.0589z^{-7} \end{aligned} \tag{36}$$

$$\begin{aligned} S(z^{-1}) = {} & 1 - 0.978z^{-1} - 0.277z^{-2} + 0.369z^{-3} + 0.0018z^{-4} \\ & -0.0539z^{-5} - 0.0607z^{-6} + 4.074z^{-7} \end{aligned} \tag{37}$$

$$T(z^{-1}) = 0.17298 \tag{38}$$

The shaping of all closed loop sensitivity functions was achieved, as shown in Figure 13. It should be noted that all these functions satisfied all of the constraints mentioned above. After designing the RST controller, it was combined with the inverse LSSVM model to achieve good trajectory tracking in the presence of disturbances and improve control performance.

The four test reference signals used in modeling were also used to evaluate the effectiveness of the proposed control scheme. The experimental results of the proposed hybrid controller are shown in Figures 14 and 15. These figures compare the desired input with the output displacement of the considered piezoelectric stage. The output of the controlled piezoelectric stage showed good tracking and achieved a highly linear relationship with the desired displacement curve. The RMSEs corresponding to the test inputs D, E, F, and G were 0.0182, 0.0219, 0.0162, and 0.0227 µm, respectively. These errors accounted for 0.0520, 0.0626, 0.0463, and 0.0649% of the travel range, which indicated that the RST-LSSVM controller had greater enhancement of tracking capabilities. To further evaluate the generalization ability of the proposed control scheme, four new datasets (H, I, J, and K) with different amplitudes and frequencies were also considered. Figure 16 shows the experimental results, where the proposed control scheme tracks the new desired trajectories with satisfactory performance. The RMSEs of the test inputs H, I, J, and K were 0.0164, 0.0158, 0.0187, and 0.0181 µm, respectively, which accounted for 0.0469, 0.0451, 0.0534, and 0.0517% of the travel range, respectively. Figure 17 shows much closer relationships to the

desired linear relationship on all test inputs. These results have been compared with those obtained from the PID-LSSVM controller that was proposed in our previous work [25]. The comparison results are shown in Tables 4 and 5. The proposed RST-LSSVM control scheme had smaller RMSEs than the PID-LSSVM control scheme. Although the difference in mean RMSE values, presented in Tables 4 and 5, was small (3.4 and 7.1 nm, respectively), this small difference is considerable in ultra-precise positioning applications, such as in microscopy. In addition, the difference in RMSE values with some datasets (E, H, I, and K) is obvious (4.8, 6.9, 12.3, and 8.3 nm respectively), which demonstrates the performance improvements with the proposed control scheme. The mean values for all test inputs used in this study were also calculated, and it was found that the RST-LSSVM controller gave an improved mean value (18.6 nm) compared with the PID-LSSVM controller (23.8 nm). Figures 18 and 19 compare the obtained results in terms of position tracking errors over time. Better positioning precision was achieved with the proposed RST-LSSVM control scheme compared with the PID-LSSVM control scheme.

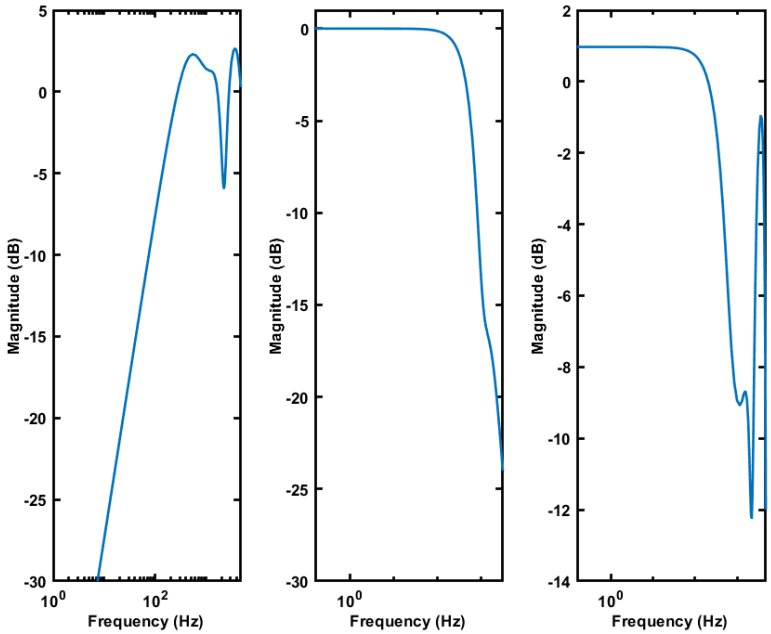

Figure 13. Closed loop sensitivity functions of the proposed RST control design: (**a**) output sensitivity function; (**b**) complementary sensitivity function; and (**c**) input sensitivity function.

Table 4. Comparison of tracking control with PID-LSSVM approach on test data D, E, F, and G.

Model	RMSE (μm)				Mean	Mean Percentage % to Travel Range
	Data D	Data E	Data F	Data G		
PID-LSSVM	0.0214	0.0267	0.0195	0.0250	0.0232	0.0663%
RST-LSSVM	0.0182	0.0219	0.0162	0.0227	0.0198	0.0566%

Table 5. Comparison of tracking control with PID-LSSVM approach on test data H, I, J, and K.

Model	RMSE (μm)				Mean	Mean Percentage % to Travel Range
	Data H	Data I	Data J	Data K		
PID-LSSVM	0.0233	0.0281	0.020	0.0264	0.0244	0.0697%
RST-LSSVM	0.0164	0.0158	0.0187	0.0181	0.0173	0.0494%

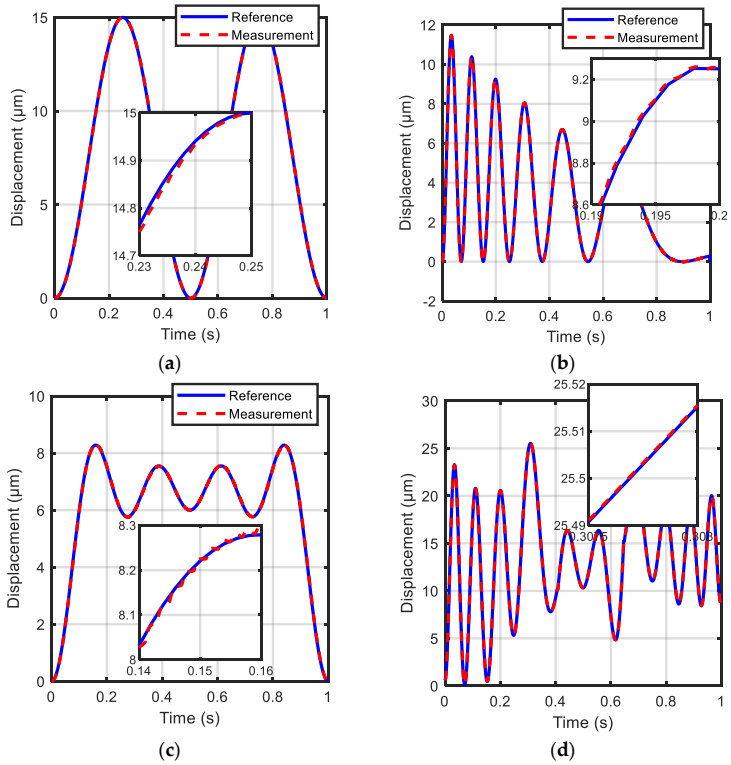

Figure 14. Experimental results of reference tracking in a closed loop with RST control and LSSVM compensation. These results were obtained by: (**a**) test reference D; (**b**) test reference E; (**c**) test reference F; and (**d**) test reference G.

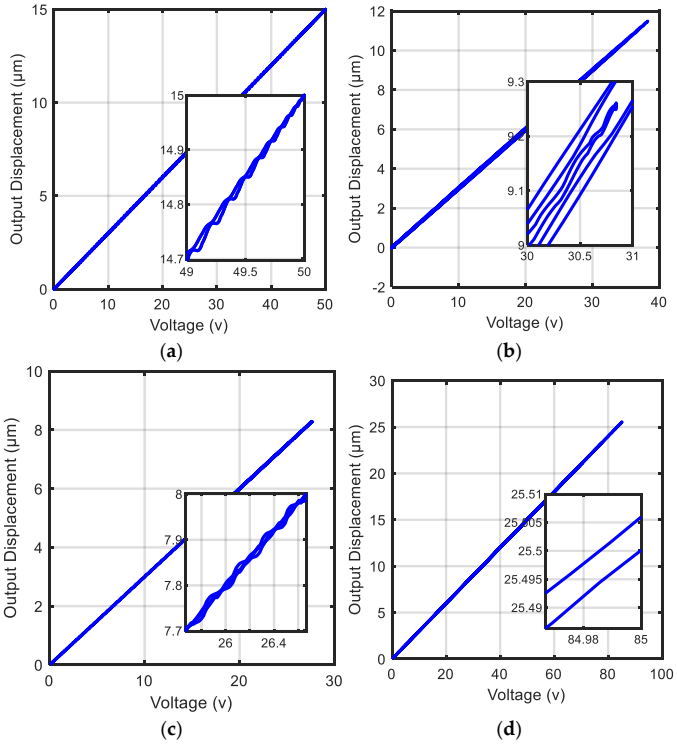

Figure 15. The effect of the proposed control scheme on hysteresis loops of the considered piezoelectric actuator. The loops shown were obtained by: (**a**) test reference D; (**b**) test reference E; (**c**) test reference F; and (**d**) test reference G.

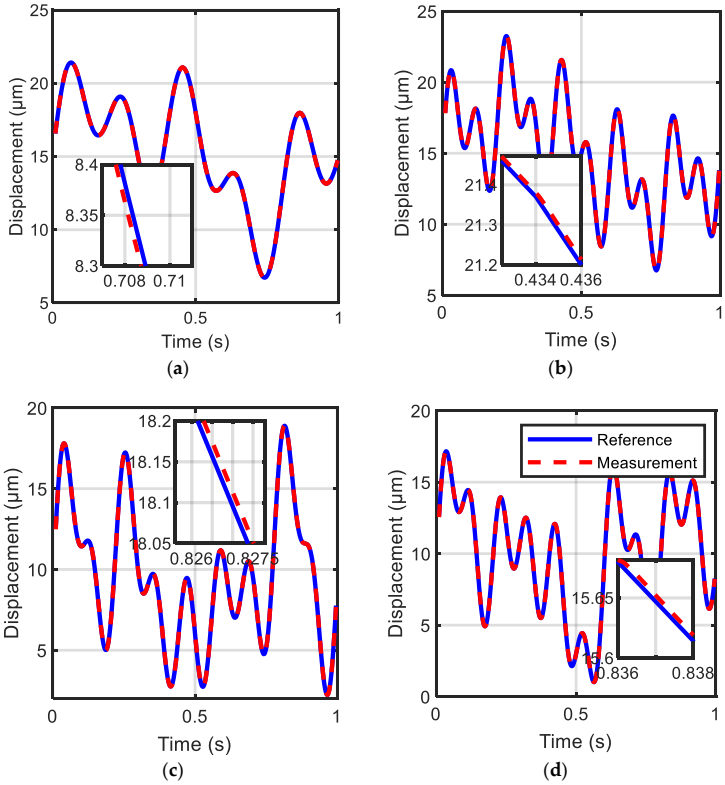

Figure 16. Experimental results of reference tracking in a closed loop with RST control and LSSVM compensation corresponding to: (**a**) test reference H; (**b**) test reference I; (**c**) test reference J; and (**d**) test reference K.

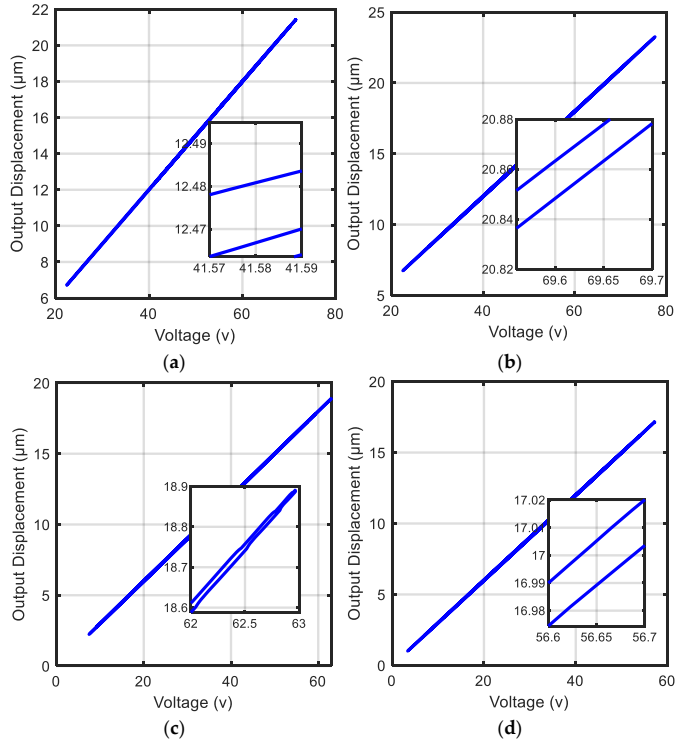

Figure 17. The effect of the proposed control scheme on hysteresis loops of the considered piezoelectric actuator. The loops shown were obtained by: (**a**) test reference H; (**b**) test reference I; (**c**) test reference J; and (**d**) test reference K.

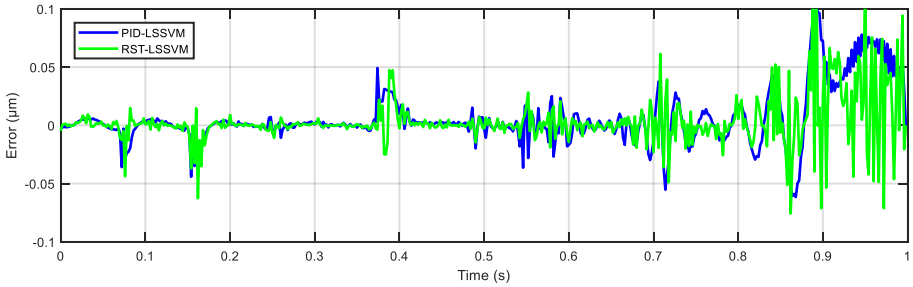

Figure 18. Tracking errors of the RST-LSSVM control scheme compared with the PID-LSSVM control scheme on data E.

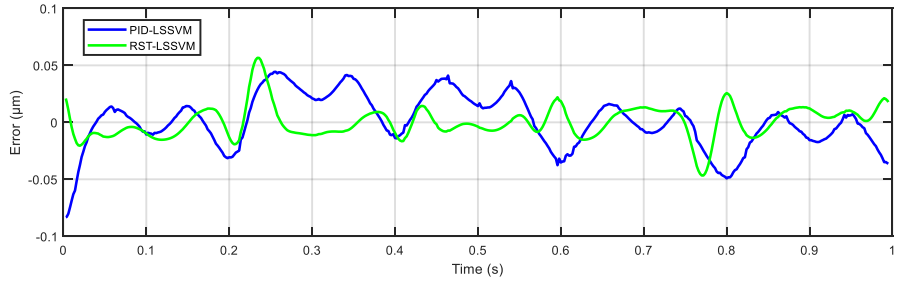

Figure 19. Tracking errors of the RST-LSSVM control scheme compared with the PID-LSSVM control scheme on data I.

To evaluate the effectiveness of our proposed control scheme, we compared our achieved results with those obtained by other control schemes (mentioned in the literature review of this paper) for the piezoelectric platform. Comparison results are presented in Table 6, where it is shown that our proposed scheme had better results compared with the other control methods. The average root mean square error obtained by the improved Preisach model [12] was 0.15 μm, which was better than those obtained by the recurrent neural networks [15] (0.465 μm) and the LSSVM algorithm approach without modeling hysteresis inverse [50] (0.62 μm). The control method that was based on the LSSVM-NARX algorithm [19] had satisfactory performance, with an average RMSE of 0.03 μm; however, the performance with LSSVM based on the stop operator and incremental PID was superior [25] (0.0238 μm). Indeed, our proposed method, which used the inverse LSSVM model combined with the hysteresis operators and RST controller, was more accurate, achieving the lowest average tracking error (RMSE of 0.0186 μm) compared with the other methods. These results indicate that the proposed control method presented in this paper has a high generalization ability to track different trajectories with different amplitudes and frequencies, as well as high tracking performance in the presence of disturbances.

Table 6. Comparison between the proposed method and previous studies.

Contributor	Method	RMSE
Qingsong Xu [50]	Feedforward–feedback scheme based on the least squares support vector machine without modeling hysteresis inverse.	0.62
Yongcheng Xiong et al. [15]	Control scheme based on recurrent neural networks.	0.465
Wei Tech Ang et al. [12]	Control scheme based on the improved Preisach.	0.15
Liangsong Huang et al. [19]	Feedforward–feedback scheme based on the least squares support vector machine, combined with NARX model and PID controller.	0.03
PID-LSSVM [25]	Feedforward–feedback scheme based on particle swarm optimization and least squares support vector machine, combined with discrete memory (stop operators) and incremental PID controller.	0.0238
The proposed RST-LSSVM	Feedforward–feedback scheme based on particle swarm optimization and least squares support vector machine, combined with discrete memory (stop operators) and RST controller.	0.0186

6. Conclusions

This paper presents a hybrid control strategy for a piezoelectric actuator. The authors used a kernel-based learning method to design the feedforward controller, and pole placement with sensitivity function shaping methodology was used to design a digital RST feedback controller. The feedforward controller was constructed employing an inverse model using a stop operator to solve the multi-mapping problem while its parameters were identified using the PSO-LSSVM algorithm. The simulation results demonstrated that the PSO-LSSVM model produced high modeling accuracy (RMSE: D = 0.01061, E = 0.01086, F = 0.0123, and G = 0.0126 μm), with a reduced number of stop operators (n = 55). The feasibility of the proposed control strategy was investigated using a nanopositioning platform. The experimental results showed that the inverse LSSVM model could effectively track the desired displacement. The remaining errors caused by modeling errors and the disturbance effect were addressed by a RST feedback controller. The results showed that the proposed hybrid control strategy outperformed the PID-LSSVM control strategy in terms of robustness and generalizing ability from controlling the rate-dependent hysteresis effect (RSME: D = 0.0182, E = 0.0219, F = 0.0162, G = 0.0227, H = 0.0164, I = 0.0158, J = 0.0187, and K = 0.0181 μm). The mean of tracking errors obtained from all test datasets with the PID-LSSVM controller was 0.0238 μm, whereas the RST-LSSVM controller achieved 0.0186 μm.

A high-speed controller is required in applications that require high-speed positioning in real time. This can be done by solving the computational complexity problem. This task becomes very difficult for multi-axes nanopositioning applications. The universality of our proposed control method should be examined with more experiments on other types of piezoelectric actuators. These issues should be examined further in future research.

Author Contributions: Conceptualization, A.G.B. and I.A.; methodology, A.G.B. and I.A.; software, A.G.B.; validation, A.G.B.; formal analysis, A.G.B. and I.A.; investigation, A.G.B. and I.A.; resources, I.A. and A.A.; data curation, A.G.B. and I.A.; writing—original draft preparation, A.G.B.; writing—review and editing, I.A. and Y.B.S.; supervision, I.A.; project administration, I.A., Y.B.S. and A.A.; funding acquisition, Y.B.S. All authors have read and agreed to the published version of the manuscript.

Funding: Research was funded by King Saud University through Researchers Supporting Project number (RSP-2021/270), King Saud University, Riyadh, Saudi Arabia.

Institutional Review Board Statement: Not applicable.

Informed Consent Statement: Not applicable.

Data Availability Statement: All data are available in the manuscript.

Conflicts of Interest: The authors declare no conflict of interest.

References

1. Ewing, J.A. X. Experimental researches in magnetism. *Philos. Trans. R. Soc. Lond.* **1885**, *176*, 523–640.
2. Gan, J.; Zhang, X. A review of nonlinear hysteresis modeling and control of piezoelectric actuators. *AIP Adv.* **2019**, *9*, 40702. [CrossRef]
3. Gu, G.-Y.; Zhu, L.-M.; Su, C.-Y.; Ding, H.; Fatikow, S. Modeling and control of piezo-actuated nanopositioning stages: A survey. *IEEE Trans. Autom. Sci. Eng.* **2014**, *13*, 313–332. [CrossRef]
4. Sabarianand, D.V.; Karthikeyan, P.; Muthuramalingam, T. A review on control strategies for compensation of hysteresis and creep on piezoelectric actuators based micro systems. *Mech. Syst. Signal Process.* **2020**, *140*, 106634. [CrossRef]
5. Al Janaideh, M.; Rakheja, S.; Su, C.-Y. Experimental characterization and modeling of rate-dependent hysteresis of a piezoceramic actuator. *Mechatronics* **2009**, *19*, 656–670. [CrossRef]
6. Webb, G.V.; Lagoudas, D.C.; Kurdila, A.J. Hysteresis modeling of SMA actuators for control applications. *J. Intell. Mater. Syst. Struct.* **1998**, *9*, 432–448. [CrossRef]
7. Zhu, W.; Wang, D.-h. Non-symmetrical Bouc–Wen model for piezoelectric ceramic actuators. *Sens. Actuators A Phys.* **2012**, *181*, 51–60. [CrossRef]
8. Ji, H.; Lv, B.; Ding, H.; Yang, F.; Qi, A.; Wu, X.; Ni, J. Modeling and Control of Hysteresis Characteristics of Piezoelectric Micro-Positioning Platform Based on Duhem Model. *Actuators* **2022**, *11*, 122. [CrossRef]

9. Xiao, S.; Li, Y. Modeling and high dynamic compensating the rate-dependent hysteresis of piezoelectric actuators via a novel modified inverse Preisach model. *IEEE Trans. Control. Syst. Technol.* **2012**, *21*, 1549–1557. [CrossRef]
10. Zhou, C.; Feng, C.; Aye, Y.N.; Ang, W.T. A digitized representation of the modified Prandtl–Ishlinskii hysteresis model for modeling and compensating piezoelectric actuator hysteresis. *Micromachines* **2021**, *12*, 942. [CrossRef]
11. Meng, Y.; Wang, X.; Li, L.; Huang, W.; Zhu, L. Hysteresis Modeling and Compensation of Piezoelectric Actuators Using Gaussian Process with High-Dimensional Input. *Actuators* **2022**, *11*, 115. [CrossRef]
12. Yang, L.; Ding, B.; Liao, W.; Li, Y. Identification of Preisach Model Parameters Based on an Improved Particle Swarm Optimization Method for Piezoelectric Actuators in Micro-Manufacturing Stages. *Micromachines* **2022**, *13*, 698. [CrossRef] [PubMed]
13. Liu, D.; Fang, Y.; Wang, H. Intelligent rate-dependent hysteresis control compensator design with Bouc-Wen model based on RMSO for piezoelectric actuator. *IEEE Access* **2020**, *8*, 63993–64001. [CrossRef]
14. Ahmed, K.; Yan, P. Modeling and identification of rate dependent hysteresis in piezoelectric actuated nano-stage: A gray box neural network based approach. *IEEE Access* **2021**, *9*, 65440–65448. [CrossRef]
15. Xiong, Y.; Jia, W.; Zhang, L.; Zhao, Y.; Zheng, L. Feedforward Control of Piezoelectric Ceramic Actuators Based on PEA-RNN. *Sensors* **2022**, *22*, 5387. [CrossRef]
16. Raj, R.A.; Samikannu, R.; Yahya, A.; Mosalaosi, M. Performance evaluation of natural esters and dielectric correlation assessment using artificial neural network (ANN). *J. Adv. Dielectr.* **2020**, *10*, 2050025. [CrossRef]
17. Suykens, J.A.K.; Van Gestel, T.; De Brabanter, J.; De Moor, B.; Vandewalle, J. *Least Squares Support Vector Machines*; World Scientific Publishing: Singapore, 2002; pp. 71–100.
18. Kaytez, F.; Taplamacioglu, M.C.; Cam, E.; Hardalac, F. Forecasting electricity consumption: A comparison of regression analysis, neural networks and least squares support vector machines. *Int. J. Electr. Power Energy Syst.* **2015**, *67*, 431–438. [CrossRef]
19. Huang, L.; Hu, Y.; Zhao, Y.; Li, Y. Modeling and control of IPMC actuators based on LSSVM-NARX paradigm. *Mathematics* **2019**, *7*, 741. [CrossRef]
20. Liu, X.; Ma, Z.; Mao, X.; Shan, J.; Wang, Y. A fast and accurate piezoelectric actuator modeling method based on truncated least squares support vector regression. *Rev. Sci. Instrum.* **2019**, *5*, 055004.
21. Xu, Q. Identification and compensation of piezoelectric hysteresis without modeling hysteresis inverse. *IEEE Trans. Ind. Electron.* **2012**, *60*, 3927–3937. [CrossRef]
22. Mao, X.; Wang, Y.; Liu, X.; Guo, Y. A hybrid feedforward-feedback hysteresis compensator in piezoelectric actuators based on least-squares support vector machine. *IEEE Trans. Ind. Electron.* **2017**, *65*, 5704–5711. [CrossRef]
23. Nelles, O. *Nonlinear System Identification: From Classical Approaches to Neural Networks, Fuzzy Models, and Gaussian Processes*; Springer Nature: Berlin/Heidelberg, Germany, 2020; p. 4.
24. Farrokh, M. Hysteresis simulation using least-squares support vector machine. *J. Eng. Mech.* **2018**, *144*, 04018084. [CrossRef]
25. Baziyad, A.G.; Nouh, A.S.; Ahmad, I.; Alkuhayli, A. Application of Least-Squares Support-Vector Machine Based on Hysteresis Operators and Particle Swarm Optimization for Modeling and Control of Hysteresis in Piezoelectric Actuators. *Actuators* **2022**, *11*, 217. [CrossRef]
26. Landau, I.D. The RST digital controller design and applications. *Control Eng. Pract.* **1998**, *6*, 155–165. [CrossRef]
27. Landau, I.D.; Karimi, A. Robust digital control using pole placement with sensitivity function shaping method. *Int. J. Robust Nonlinear Control. IFAC-Affil. J.* **1998**, *8*, 191–210. [CrossRef]
28. Langer, J.; Landau, I.D. Combined pole placement/sensitivity function shaping method using convex optimization criteria. *Automatica* **1999**, *35*, 1111–1120. [CrossRef]
29. Ahmad, I.; Abdurraqeeb, A.M. Tracking control of a piezoelectric actuator with hysteresis compensation using RST digital controller. *Microsyst. Technol.* **2017**, *23*, 2307–2317. [CrossRef]
30. Rakotondrabe, M.; Al Janaideh, M. An RST control design based on interval technique for piezomicropositoning systems with rate-dependent hysteresis nonlinearities. In Proceedings of the 2019 IEEE 58th Conference on Decision and Control (CDC), Nice, France, 11–13 December 2019; pp. 1–8.
31. Abdurraqeeb, A.M.; Al-Shamma'a, A.A.; Alkuhayli, A.; Noman, A.M.; Addoweesh, K.E. RST Digital Robust Control for DC/DC Buck Converter Feeding Constant Power Load. *Mathematics* **2022**, *10*, 1782. [CrossRef]
32. Ali, Z.A.; Li, X. Controlling of an under-actuated quadrotor UAV equipped with a manipulator. *IEEE Access* **2020**, *8*, 34664–34674. [CrossRef]
33. Physik Instrumente. P-752 High-Precision Nanopositioning Stage. Available online: https://www.physikinstrumente.com/en/products/nanopositioning-piezo-flexure-stages/linear-piezo-flexure-stages/p-752-high-precision-nanopositioning-stage-200800/ (accessed on 14 July 2022).
34. Physik Instrumente. E-505 Piezo Amplifier Module. Available online: https://www.physikinstrumente.com/en/products/controllers-and-drivers/nanopositioning-piezo-controllers/e-505-piezo-amplifier-module-602300/ (accessed on 15 July 2022).
35. dSPACE. DS1104 R&D Controller Board. Available online: https://www.dspace.com/en/inc/home/products/hw/singbord/ds1104.cfm (accessed on 14 July 2022).
36. Lai, X.; Pan, H.; Zhao, X. Adaptive control for pure-feedback nonlinear systems preceded by asymmetric hysteresis. *Energies* **2019**, *12*, 4675. [CrossRef]
37. Hu, K.; Ge, H.; Li, H.; Xie, S.; Xu, S. Rate-Dependent Hysteresis Modeling and Displacement Tracking Control Based on Least-Squares SVM for Axially Pre-Compressed Macro-Fiber Composite Bimorph. *Materials* **2022**, *15*, 6480. [CrossRef] [PubMed]

38. Zhang, J.; Wang, X.; Shao, X. Design and real-time implementation of Takagi–Sugeno fuzzy controller for magnetic levitation ball system. *IEEE Access* **2020**, *8*, 38221–38228. [CrossRef]
39. Mayergoyz, I. Mathematical models of hysteresis. *IEEE Trans. Magn.* **1986**, *22*, 603–608. [CrossRef]
40. Brokate, M.; Sprekels, J. *Hysteresis and Phase Transitions*; Springer: New York, NY, USA, 1996; pp. 52–105.
41. Suykens, J.A.; Vandewalle, J.; De Moor, B. Optimal control by least squares support vector machines. *Neural Netw.* **2001**, *14*, 23–35. [CrossRef]
42. Eberhart, R.C.; Shi, Y.; Kennedy, J. *Swarm Intelligence*; Elsevier: Amsterdam, The Netherlands, 2001; pp. 287–324.
43. Kennedy, J.; Eberhart, R. Particle swarms optimization. In Proceedings of the IEEE International Conference on Neural Networks, Perth, Australia, 27 November–1 December 1995; Volume 4.
44. Mueller, A. (Ed.) *Recent Advances in Robust Control-Novel Approaches and Design Methods*; IntechOpen: London, UK, 2011; pp. 341–360.
45. Li, Z.; Shan, J.; Gabbert, U. A direct inverse model for hysteresis compensation. *IEEE Trans. Ind. Electron.* **2020**, *68*, 4173–4181. [CrossRef]
46. Ahmad, I.; Ali, A.E.A.; Salamah, Y.B. MIMO H μ Feedback Controller with Feedforward Compensator for Scanning Tunneling Microscope Having 3D Cross-Coupled Piezoelectric Actuator. *IEEE Access* **2021**, *9*, 153750–153766. [CrossRef]
47. De Brabanter, K.; Karsmakers, P.; Ojeda, F.; Alzate, C.; De Brabanter, J.; Pelckmans, K.; De Moor, B.; Vandewalle, J.; Suykens, J.A. *LS-SVMlab Toolbox User's Guide: Version 1.7*; Katholieke Universiteit Leuven: Leuven, Belgium, 2010.
48. Chen, Q.; Wang, G. PSO-driven micromechanical identification of in-situ properties of fiber-reinforced composites. *Compos. Struct.* **2019**, *220*, 608–621. [CrossRef]
49. Rezaee Jordehi, A.; Jasni, J. Parameter selection in particle swarm optimisation: A survey. *J. Exp. Theor. Artif. Intell.* **2013**, *25*, 527–542. [CrossRef]
50. Xu, Q.; Wong, P.-K. Hysteresis modeling and compensation of a piezostage using least squares support vector machines. *Mechatronics* **2011**, *21*, 1239–1251. [CrossRef]